

# Laser-induced disassembly of a graphene single crystal into a nanocrystalline network

B. Krauss, T. Lohmann, D.-H. Chae, M. Haluska,\* K. von Klitzing, and J. H. Smet<sup>†</sup>

*Max-Planck-Institut fuer Festkoerperforschung, Heisenbergstrasse 1, D-70569 Stuttgart, Germany*

(Received 23 December 2008; revised manuscript received 2 March 2009; published 22 April 2009)

We report about investigations of time-dependent structural modifications in single-crystal graphene due to laser irradiation even at moderate power levels of 1 mW in a diffraction-limited spot. The modifications have been characterized by *in situ* scanning confocal Raman spectroscopy, atomic force height microscopy, and transport studies. The time evolution of the Raman spectrum reveals two different effects: on a short-time scale, dopants, initially present on the flake, are removed. The longer time scale behavior points to a laser induced gradual local decomposition of single-crystal graphene into a network of interconnected nanocrystallites with a characteristic length scale of approximately 10 nm due to bond breaking. The broken bonds offer additional docking sites for adsorbates as confirmed in transport and AFM height studies. These controlled structural modifications may for instance be valuable for enhancing the local reactivity, trimming graphene based gas sensors and generating spatially varying doping patterns.

DOI: [10.1103/PhysRevB.79.165428](https://doi.org/10.1103/PhysRevB.79.165428)

PACS number(s): 81.05.Uw, 78.30.-j, 81.07.Bc

## I. INTRODUCTION

The successful isolation of graphene in 2004 (Ref. 1) has triggered tremendous research effort. An important impetus has come from the unusual linear dispersion in the band structure of graphene as it promises among others access in table top solid-state experiments to phenomena normally reserved for high-energy physics. Raman spectroscopy is a versatile and powerful tool to probe elementary excitations such as phonons, excitons, plasmons, and magnons. In a confocal arrangement, it is possible to obtain spatial Raman maps with a resolution down to the diffraction limit. Raman spectroscopy has historically played an important role in carbon based systems as it allows to distinguish the different hybridization of bonds ( $sp$ ,  $sp^2$ ,  $sp^3$ ) and extract information about disorder.<sup>2,3</sup> In layered graphite related systems with  $sp^2$  bonding, Raman data can in addition reveal the crystallite size, presence of doping<sup>4</sup> and defects.<sup>5</sup> The existence of a double-resonance mechanism even enables studies of the phase breaking length<sup>6</sup> and the distinction between various local arrangements of carbon atoms at the edge such as the zigzag or armchair configurations.<sup>7</sup> Also for graphene studies, Raman has proven a valuable tool as it allows to distinguish monolayer graphene from bilayers and multilayers. While Raman spectroscopy has usually been considered non-invasive, we will show here that laser irradiation of graphene or few-layer graphene either has to be dosed carefully to avoid structural modifications or can on purpose be exploited to induce structural changes in graphene in a controlled manner.

## II. EXPERIMENTAL ARRANGEMENT

Graphene flakes were prepared on doped Si-substrates covered with a 300 nm thick dry thermal SiO<sub>2</sub> using micro-mechanical cleavage similar to the method described in Ref. 1. Monolayers and bilayers were identified with Raman spectroscopy<sup>8</sup> as well as optical microscopy through a calibration of the black-white contrast as proposed in Ref. 9. The results described here focus on monolayers. Comparable re-

sults were obtained on bilayer graphene. The effects become however substantially weaker as the number of layers grows. They are absent in bulk highly oriented pyrolytic graphite (HOPG) even at the maximum laser power of 12 mW. The measurements were performed on a combined atomic force microscope (AFM) and scanning confocal Raman setup using wavelengths of 488.0 nm from an argon-ion laser or 632.8 nm from a He-Ne laser and power levels up to 12 mW. The integrated high numerical aperture optics allows a diffraction-limited spot size with a diameter of approximately 400 nm on the sample for 488 nm laser light. The sample is mounted on a 100×100 μm<sup>2</sup> piezo scanner. Alternatively, the incident laser beam can be deflected by a piezo-driven mirror within an 80×80 μm<sup>2</sup> range. The reflected light can be analyzed either by a photo multiplier tube or a Raman spectrometer with a peak-to-peak resolution of up to 1 cm<sup>-1</sup>. An AFM-tip can be installed in the vicinity of the laser spot to allow AFM and Raman measurements at the same location.

## III. RAMAN SPECTRUM AND LASER EXPOSURE

### A. Overview

Figure 1 shows a typical Raman spectrum obtained on a freshly prepared flake with a diffraction-limited 1 mW laser spot of 488 nm wavelength after an acquisition time of 30 s. The following Raman features can be distinguished: the first observable peak appears at  $\approx 1590$  cm<sup>-1</sup> and is associated with the zone-center in-plane longitudinal optical phonons (middle inset in Fig. 1 and Ref. 10). This well-known  $G$  peak is characteristic for  $sp^2$ -hybridized carbon-carbon bonds. The second prominent peak is located at  $\approx 2700$  cm<sup>-1</sup>. This  $2D$  peak originates from a double-resonance process.<sup>11</sup> The incoming laser light creates an electron-hole pair and after two inelastic-scattering events involving phonons with opposite momenta Raman light is emitted during recombination (right inset in Fig. 1). If defects are present, one of the two scattering events can occur elastically (left inset in Fig. 1). This yields the defect or  $D$  peak. The  $D$  peak exhibits only half

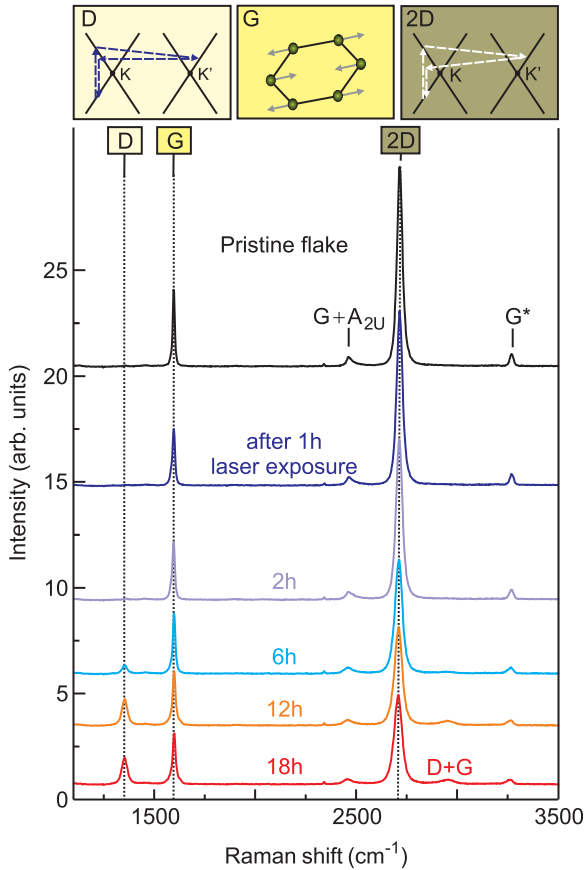


FIG. 1. (Color) Laser-induced change in the Raman spectrum. The black line (offset in intensity for clarity) is the spectrum of a pristine graphene monolayer. Other Raman spectra were obtained after laser exposure with 1 mW for the time interval indicated near each trace. Comparing the Raman spectrum after 18 h laser exposure with the spectrum of the pristine flake reveals dramatic changes. The appearance of the  $D$  peak as well as the decrease in the  $G$  and  $2D$  peak intensities are signatures of structural modifications.

the Raman shift. An increase in the number of defects, would result in an increase of the  $D$  peak intensity and a concomitant drop in the intensity of the  $2D$  peak. The  $D$  peak is not observable in our pristine flake, which attests the good crystalline quality and undetectable small concentration of defects. A shape analysis of the  $2D$  peak has been successfully used to distinguish single layers from bilayers or multilayers.<sup>8</sup> For monolayer graphene the  $2D$  peak can be fitted to a single Lorentzian while the multiple bands in multilayer graphene give rise to a more complex peak structure that requires for instance fitting to 4 Lorentzians for bilayers. Here, the  $2D$  peak clearly indicates that the flake is a monolayer. Additional smaller features in the Raman spectrum have been identified as well and were labeled in Fig. 1, but are not relevant for the remaining discussions ( $G^*$  at  $3250\text{ cm}^{-1}$ , which results from an intravalley double-resonance scattering process, and the  $G+A_{2U}$  peak at  $2460\text{ cm}^{-1}$ ).

Figure 1 also plots Raman spectra after the graphene flake has been exposed to the diffraction-limited focused laser spot with an intensity of 1 mW for different time intervals. The

Raman spectrum changes drastically with time. After 18 h (bottom red line in Fig. 1) a strong  $D$  peak at  $1350\text{ cm}^{-1}$  has emerged. It indicates a large increase in the number of broken  $sp^2$  carbon-carbon bonds.<sup>5</sup> Concomitantly a peak has appeared at approximately  $2950\text{ cm}^{-1}$  or a Raman shift equal to the sum of the  $G$  and  $D$  peak Raman shifts. This combined  $D+G$  peak is in general only observed in the vicinity of defects. We note also the drop in intensity of the  $2D$  peak. The presence of defects also allows the double-resonance mechanism with only one inelastic event and the  $D$  peak grows at the expense of the  $2D$  peak, which involves two inelastic events. The  $2D$  peak of the treated flake remains composed of a single Lorentzian despite the apparent local structural modifications of the flake. We point out that the Raman spectrum obtained after 18 h of laser exposure is very different from that of amorphous carbon,<sup>12</sup>  $sp^3$ -bonded diamond,<sup>13</sup> and graphite oxide.<sup>14</sup>

### B. Time resolved Raman measurements

In order to gain more insight into these laser induced modifications, we have performed time-resolved Raman measurements. The laser power was set to a moderate level of 1 mW and the laser spot was focused down to about 500 nm. A Raman spectrum was recorded every 30 s. During a time interval of 18 h spectra were acquired. These spectra were analyzed with respect to the intensity and location of the three most prominent features: the  $G$ ,  $D$  and  $2D$  peaks. To improve the signal-to-noise ratio, a signal-averaging procedure was applied to the extracted data traces. It consisted of a fast Fourier transform (FFT), followed by the removal of high-frequency components via a parabolic low-pass filter with its maximum at zero frequency and zero transmission beyond the cutoff frequency defined by  $\frac{1}{(mt)}$ . The data were then back transformed. Here,  $t$  refers to the time interval in between two recorded spectra and  $m$  was set equal to 36.

Figures 2(a) and 2(b) display the time dependence of the  $G$  peak intensity and position. The intensity initially exhibits a rapid drop. So does the peak position. Both traverse a local minimum after 2 h. After 5 h the intensity decreases monotonously, while the location of the  $G$  peak continues to rise. We will argue that two processes, which occur simultaneously but on different time scales, can account for this behavior. Laser-induced heating is held responsible for the removal of dopants. It causes a drop of the  $G$  peak position and dominates the Raman spectrum initially in the region denoted as regime I in Fig. 2(b). Previously, it was shown that laser irradiation may cause heating of the electronic system.<sup>15</sup> This should be distinguished from the removal of adsorbates due to laser heating as described here. While dopants continue to be removed, the longer term behavior is mainly attributed to  $sp^2$ -carbon-carbon bond breaking and the gradual disassembly of the macroscopic single graphene crystal into a network of interconnected graphene nanocrystallites at the location of the laser spot [regime II in Fig. 2(b)]. The time evolution of other Raman features also corroborates this interpretation as will be discussed later.

### C. Influence of doping on the Raman spectrum

We first consider the influence of removing doping adsorbates on the Raman spectrum. It has been demonstrated pre-

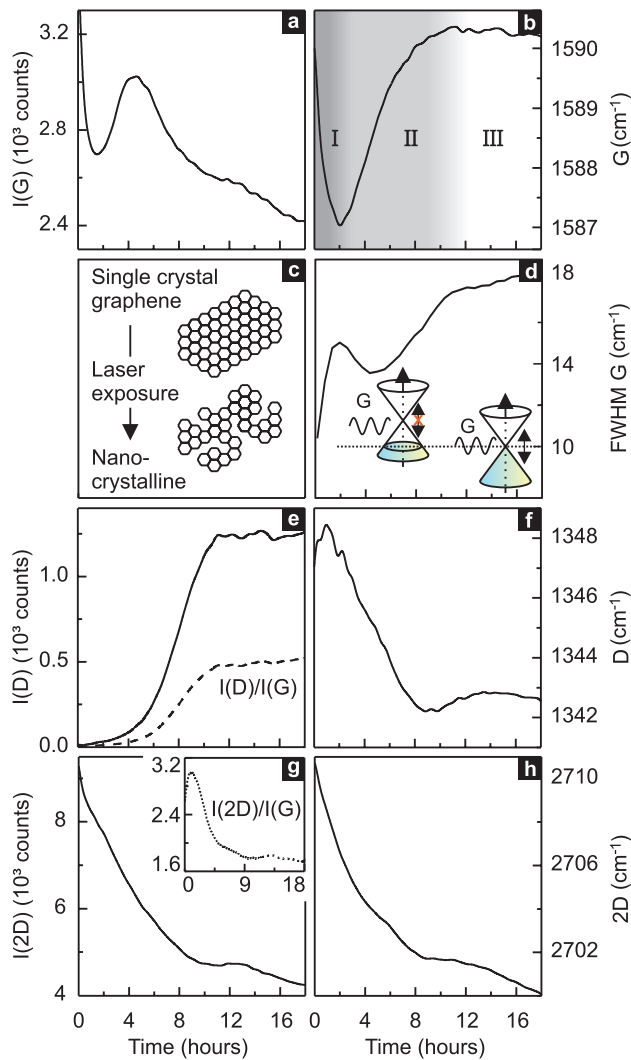


FIG. 2. (Color) Time evolution of the  $G$ ,  $D$ , and  $2D$  Raman peaks. Panels (a), (e), and (g) show the intensity of these peaks as a function of time during laser exposure with 1 mW of power and a wavelength of 488 nm. For each data point on these curves a Raman spectrum was acquired in the range from 1024 to 3770  $\text{cm}^{-1}$  with a 30 s integration time. In panel (e) also the intensity ratio between the  $D$  and  $G$  peaks has been included as well as the intensity ratio between the  $2D$  and  $G$  peak [inset in panel (g)]. Panels (b), (f), and (h) display the time development of the position of each of these Raman peaks. The FWHM of the  $G$  peak is given in (d). The observed changes with time suggest a structural modification of a single crystal of graphene into a network of graphene nanocrystallites as depicted in a cartoonlike fashion in panel (c).

viously through the field effect that the  $G$  peak undergoes a redshift as the carrier density drops.<sup>16</sup> In graphene the adiabatic Born-Oppenheimer approximation is not valid. The charge-carrier density  $n$  enters the electron phonon coupling<sup>4</sup> and causes phonon softening when  $n$  decreases. The initial behavior of the  $G$  peak [see Fig. 2(b)], i.e., both the sign and magnitude of the change in the Raman shift, is consistent with a drop in the charge-carrier density due to the removal of dopant molecules. Laser heating is presumably responsible for the dopant removal. The behavior is analogous to the influence of heating with a resistor in close thermal con-

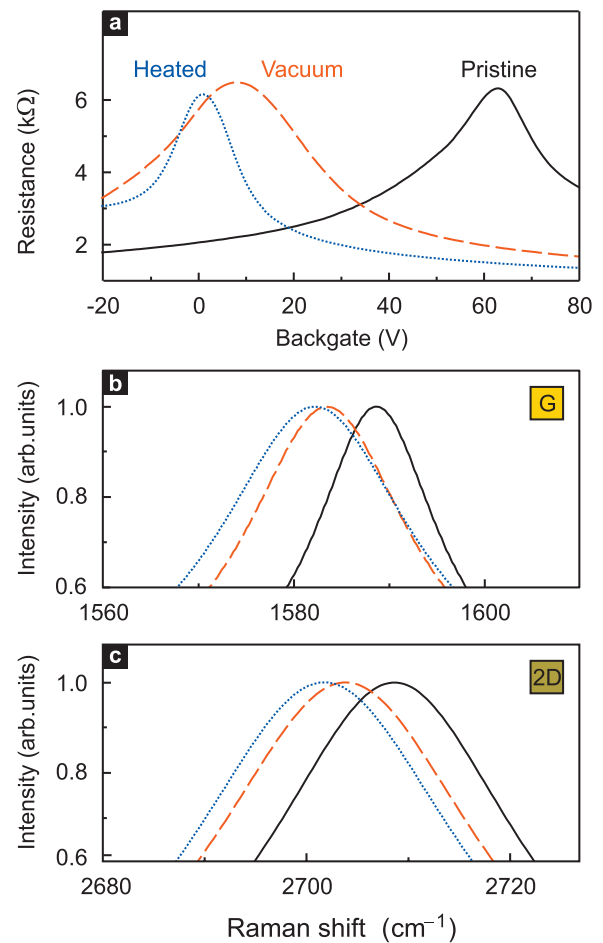


FIG. 3. (Color) Influence of removing dopants on the Raman spectrum of graphene. (a) field-effect curve, (b)  $G$  Raman peak, and (c)  $2D$  Raman peak of the as prepared flake (black solid lines), after evacuating the sample for 90 min (red dashed lines) and after heating the sample to 110  $^{\circ}\text{C}$  in vacuum (blue dotted trace). Removal of dopants causes a redshift of the  $G$  as well as  $2D$  peak.

tact under vacuum conditions as shown in Fig. 3 by combining Raman studies with transport studies on a sample with patterned Ohmic contacts.

The initial doping level of the as prepared graphene flake without special treatment was determined from the charge neutrality point at 63 V to be about  $5 \times 10^{12}$  holes/ $\text{cm}^2$  when measuring the field-effect transport characteristic [Fig. 3(a), solid black line]. Subsequently, the  $G$  and  $2D$  Raman features were recorded [Figs. 3(b) and 3(c), solid black line]. The carrier density, i.e., dopant concentration, was determined again after removing dopants by evacuating the sample chamber during a time period of 90 min. The carrier density dropped to  $7 \times 10^{11}$   $\text{cm}^{-2}$  [red dashed line in Fig. 3(a), the back-gate voltage at the charge neutrality point now equals  $\approx 9$  V]. The Raman spectra around the  $G$  and  $2D$  features are again plotted in Figs. 3(b) and 3(c) (red dashed lines) and exhibit a redshift. Finally the sample was heated in vacuum up to 110  $^{\circ}\text{C}$ . It reduced the doping concentration further until the Dirac point was close to zero back-gate voltage. This additional reduction in the carrier density is again reflected in the Raman spectrum as a redshift [blue dotted

TABLE I. Raman peak positions of the  $G$  and  $2D$  peak depending on the charge-carrier density  $n$ .

	$n$ ( $\text{cm}^{-2}$ )	$G$ peak ( $\text{cm}^{-1}$ )	$2D$ peak ( $\text{cm}^{-1}$ )
Pristine	$4.9 \times 10^{12}$	$1588.7 \pm 0.1$	$2709.3 \pm 0.1$
Vacuum	$7.0 \times 10^{11}$	$1583.6 \pm 0.7$	$2704.4 \pm 0.2$
Heated	$7.8 \times 10^{10}$	$1582.3 \pm 2.0$	$2702.0 \pm 0.3$

traces in Figs. 3(b) and 3(c)]. The peak positions are listed in Table I. They are obtained from fitting the experimental data with Lorentzians. The  $G$  peak position and its shift with density agree well with the experimental data based on field-effect tuning of the density previously reported for instance in Ref. 17:  $1589.5 \pm 0.8 \text{ cm}^{-1}$  for  $n=5 \times 10^{12} \text{ cm}^{-2}$  and  $1583.5 \pm 1.2 \text{ cm}^{-1}$  for  $n=7 \times 10^{11} \text{ cm}^{-2}$ .

Figure 3 also shows that a drop in the carrier density causes a redshift of the  $2D$  peak as well. This behavior of the  $G$  and  $2D$  peaks associated with the removal of dopants is also seen in the experiment of Fig. 2(h) when the graphene flake is exposed to laser radiation. Since the flake is measured under ambient conditions water and oxygen are believed to be among the dominant doping species. The intensity ratio of the  $2D$  peak and the  $G$  peak  $I(2D)/I(G)$  is related to the charged impurity concentration in graphene.<sup>18–20</sup> The higher the graphene is doped, the lower is this ratio. For regime I, we find that  $I(2D)/I(G)$  increases. This further corroborates that dopants are removed by the laser beam in regime I.

Additional evidence that the initial rapid time dependence of the Raman features is caused by dopant removal comes from the time evolution of the full width at half maximum (FWHM) of the  $G$  peak shown in Fig. 2(d). At time zero the FWHM equals approximately  $10.5 \text{ cm}^{-1}$ . It ascends steeply within the first 2 h of laser exposure up to  $15.2 \text{ cm}^{-1}$ . This rise in the FWHM is correlated with the drop of the  $G$  peak position. The left inset schematically highlights the case with large  $p$  doping. At high doping levels, the energy of the  $G$  phonon ( $\approx 200 \text{ meV}$ ) is insufficient to create an electron-hole (e-h)-pair as there are no occupied states available. Consequently, the phonon has a long life time and the Raman peak is expected to be narrow.<sup>21</sup> In the case of low doping [right cone in Fig. 2(d)] the phonon can decay rapidly in an e-h-pair and the FWHM will grow as the charge-carrier density drops. This behavior is indeed born out in the experimental data of Fig. 2(d).

For exposure times longer than 2 h, the FWHM varies more slowly. There is an overall but much slower tendency to increase. Its value remains within a band of  $2 \text{ cm}^{-1}$  of the value reached after the initial steep ascend. Most of all, the correlation between the behavior of the  $G$  peak position and its FWHM is expected when variations in the charge-carrier density would dominate is absent. The  $G$  peak moves to larger values, which suggests an increase in the carrier density, but this blueshift is neither accompanied by a corresponding drop in the line width nor by a blueshift of the  $2D$  peak. Hence, at long exposure times ( $>2 \text{ h}$ ) other mechanisms predominantly govern the time-dependent Raman behavior.

#### D. Disassembly due to bond-disruption

During the first few hours of laser exposure the amplitude of the  $D$  peak [regime I, Fig. 2(e)] remains small. It suggests that only few carbon-carbon  $sp^2$  bonds are broken. For longer laser beam exposure [regime II in Fig. 2(e),  $t > 3-4 \text{ h}$ ] however the  $D$  peak intensity rises and eventually a substantial amount of  $sp^2$ -carbon-carbon bonds apparently get cracked. We assert that the single crystal of graphene is gradually disassembled underneath the laser spot and the graphene crystal is after long laser exposure converted from a single crystal into a network of interconnected graphene nanocrystallites due to bond disruption as illustrated in Fig. 2(c). Since the photon energy is smaller than the binding energy, two photon processes might be responsible for bond breaking. The long-time scale indicates a low probability for bond breaking.

After 10 h of laser exposure the intensity of the  $D$  peak saturates [regime III in Fig. 2(b)]. The bond breaking apparently decelerates or terminates. Tuinstra and co-workers<sup>5</sup> have carried out Raman investigations on pellets composed of single crystals of graphite. The crystallite size was determined from x-ray diffraction. Their studies revealed that the characteristic length scale  $d$  of the crystallites and the ratio between the  $D$  and  $G$  peak intensity are in inverse proportion  $I(D)/I(G) \propto 1/d$ . It simply reflects that the Raman intensity of the  $D$  peak is proportional to the percentage of “boundary” in the sample. Based on the reported data, we would conclude from the  $I(D)/I(G)$  ratio observed in the experiments here [Fig. 2(e), dashed line] that the Raman signal of the laser treated graphene flake is equivalent to that of graphene nanocrystallites with a characteristic size which saturates at an average value of approximately 10 nm. Since the intensity of the  $G$  peak is now strongly affected by the crystallite size, the ratio of the  $2D$  peak intensity and the  $G$  peak intensity no longer serves as a measure for the amount of charged impurities. Below it will be shown that this picture of nanocrystallite formation is imposingly confirmed by the behavior of the  $G$  peak position [Fig. 2(b)].

The increase in the  $D$  peak intensity is accompanied by a rise of the  $G$  peak position. If due to carbon-carbon bond disruption the graphene flake locally disintegrates into a network of nanocrystalline graphene patches, it is natural to attribute this shift of the  $G$  peak to phonon confinement.<sup>22</sup> In the pristine graphene flake, the incident photons only interact with phonons that have essentially zero momentum  $q \approx 0$  in order to fulfill momentum conservation.<sup>23</sup> For nanocrystallites with size  $d$ , the Heisenberg uncertainty principle relaxes this momentum selection rule and also phonon modes with a nonzero momentum up to  $\Delta q \approx 2\pi/d$  contribute to the Raman intensity.<sup>24</sup> For an average crystallite size of 10 nm, we obtain a maximum momentum transfer  $\Delta q \approx 0.6/\text{nm}$ . The Raman-active zone-center phonon mode exhibits a positive dispersion when moving away from the zone center.<sup>25</sup> Due to the lack of experimental phonon-dispersion data for graphene, we resort to reported inelastic x-ray scattering data of graphite to estimate this energy dispersion. A linear approximation yields a slope of  $S(\text{LO}, \Gamma) \approx 13 \text{ nm}/\text{cm}$ . For 10 nm crystallites, phonon modes with an energy larger by at most  $8 \text{ cm}^{-1}$  compared with the zone-center phonon energy

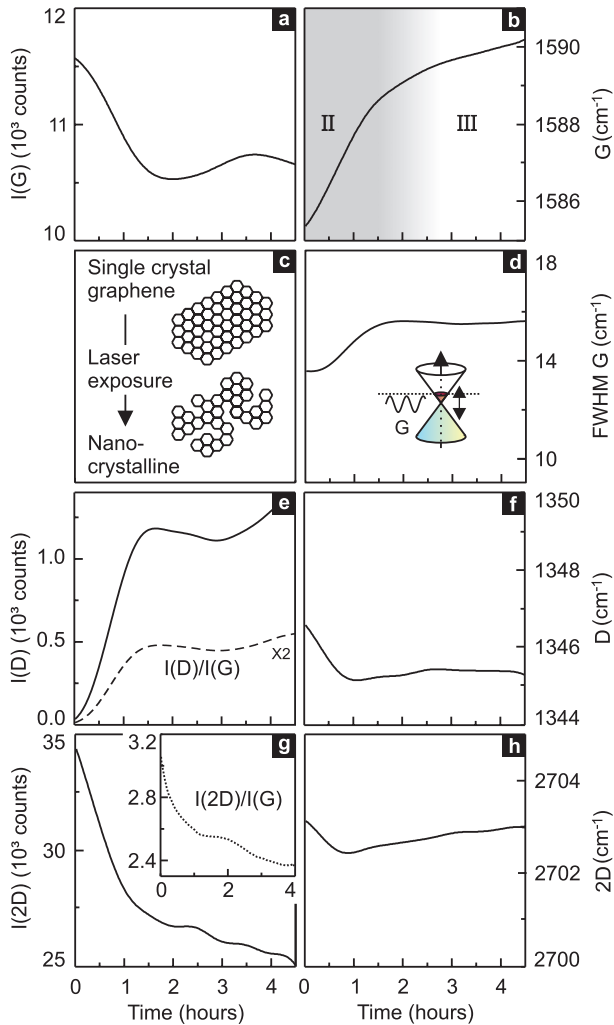


FIG. 4. (Color) Time evolution of the  $G$ ,  $D$ , and  $2D$  Raman peaks under laser exposure. Dopants have been removed by heating and pumping. Compared to Fig. 2 all features attributed to the laser induced removal of dopants are absent. The time evolution points to the disassembly of single-crystal graphene into a network of graphene nanocrystallites.

may contribute to the Raman  $G$  peak. Since all phonons with  $\Delta q$  between 0 and  $\approx 0.6/\text{nm}$  take part, the  $G$  peak will broaden. The estimated maximum blueshift is compatible with our experimental observations. We start from a highly  $p$ -doped flake with a  $G$  peak position close to  $1590\text{ cm}^{-1}$  and remove dopants by laser irradiation. The  $G$  peak position of undoped graphene is approximately  $1583\text{ cm}^{-1}$ .<sup>17</sup> The phonon confinement is expected to cause a blueshift of less than  $8\text{ cm}^{-1}$ , so that the  $G$  peak should not exceed  $1591\text{ cm}^{-1}$  in the limit of long exposure times. This agrees well with the data in Fig. 2(b). It is purely fortuitous that the initial and final  $G$  peak positions are so close.

#### IV. SEPARATION OF LASER-INDUCED RAMAN EFFECTS

In order to separate the two effects of removing dopants by laser heating and bond disruption which converts single-crystal graphene into a network of graphene nanocrystallites,

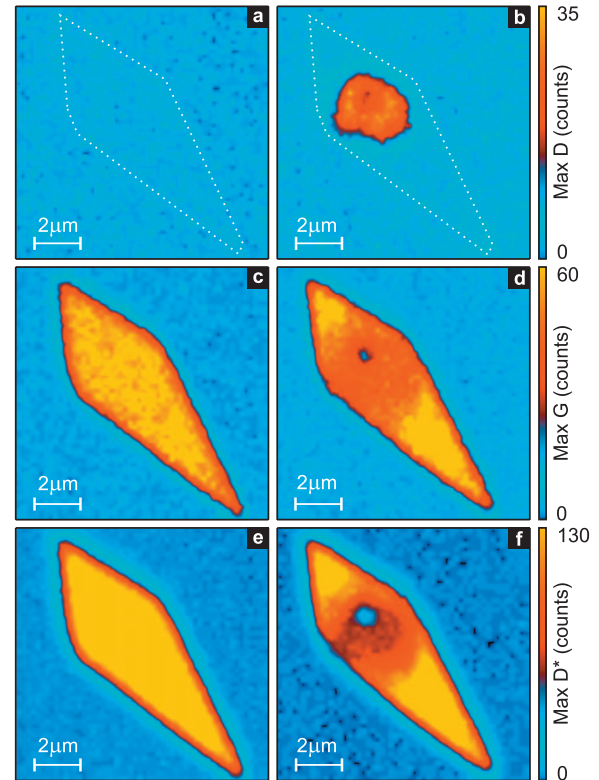


FIG. 5. (Color) Intensity maps of the  $D$ ,  $G$ , and  $2D$  Raman peaks before (left panels) and after laser exposure (right panels). (a) On the pristine flake there are virtually no defects and hence the  $D$  peak is not observable. The white dashed line is a guide to the eyes and corresponds to the border of the graphene sheet where a few defects are located. (b) Inside a circle with a diameter of approximately  $1.5\text{ }\mu\text{m}$ , the intensity of the  $D$  peak is irreversibly enhanced after laser exposure. The size and position of the spot with a large  $D$  count coincide with the laser spot. (c) Before the laser treatment, the intensity of the  $G$  peak is nearly identical across the entire graphene sheet. It confirms the high crystalline quality of the flake. (d) After laser treatment, the intensity of the  $G$  peak is reduced.

some flakes were prepared and treated so their charge neutrality point was close to zero back-gate voltage prior to laser treatment in order to minimize the influence of dopant removal. Dopants can be removed effectively either by chemical treatment of the substrate during flake preparation<sup>26</sup> or by heating the flake under vacuum conditions. These procedures to shift the charge neutrality point close to zero back-gate voltage were tested on a large series of samples and were verified by recording field-effect characteristics. Both treatments were used and led to the same results. Here we will focus on a flake annealed under vacuum conditions. The sample was heated in vacuum for several hours and subsequently kept under argon atmosphere during the time-dependent Raman experiment. The argon atmosphere ensures comparable thermal conditions as in air. The outcome of this experiment is displayed in Fig. 4. The laser exposure time serves as abscissa. Left panels show the time dependence of the Raman intensity of the  $G$ ,  $D$ , and  $2D$  peaks [Figs. 4(a), 4(e), and 4(g)]. The Raman shift of the  $G$ ,  $D$ , and  $2D$  peak as a function of time is displayed in the right panels [Figs. 4(b), 4(f), and 4(h)]. The measurement and evaluation of the data

were performed in the same manner as for collecting the data plotted in Fig. 2. One exception is the incident laser power. It was increased from 1 to 12 mW. A factor of 2 is lost in the Raman signal intensity when the sample is mounted in a chamber with a window. Hence, compared with Fig. 2 the data in Fig. 4 were effectively recorded for a six times higher intensity. The 3 h time scale in Fig. 4 is therefore comparable to the 18 h in Fig. 2.

All the time-dependent features previously attributed to the removal of dopants such as the redshift of the  $G$ ,  $D$ , and  $2D$  peaks as well as the strong increase in the FWHM of the  $G$  peak have vanished almost entirely (regime I in Fig. 2). Furthermore, the ratio  $I(2D)/I(G)$  does not increase. This again strongly supports our assertion that the Raman behavior in regime I of Fig. 2 is related to the removal of dopants by laser heating. What remains are mainly those modifications in the spectrum previously attributed to  $sp^2$  carbon-carbon bond breaking (regime II in Fig. 2 and Fig. 4): (i) a blueshift of the  $G$  peak due to phonon confinement, (ii) an increase of the  $D$  peak intensity due to the creation of additional boundaries, (iii) a decrease in the  $2D$  peak intensity, which is closely linked to (ii) as well as (iv) a reduction in the  $G$  peak amplitude as a result of the drop in the number of intact carbon-carbon bonds. The intensity ratio of the  $D$  and  $G$  peak in Fig. 4(e) (regime III, dashed line) is approximately 1/4 from which an average crystallite size of 20 nm can be estimated.<sup>5</sup> The resulting phonon confinement allows phonons with an energy larger by  $4\text{ cm}^{-1}$  to contribute to the  $G$  peak. This fits well with the experimental data in Fig. 4(b). Also the  $G$  peak is broadened due to the relaxed momentum selection rule. For the sake of completeness, we point out that some small influence from adsorbates remains present in the data of these pretreated flakes. The small decrease in the position of the  $D$  and  $2D$  peaks during the first hour is likely associated with adsorbate removal.

## V. SPATIALLY RESOLVED RAMAN SPECTROSCOPY

For the sake of completeness, Fig. 5 displays spatial maps of the  $D$ ,  $G$ , and  $2D$  peak intensities. The panels on the left are Raman maps for the pristine flake while panels on the right side were recorded after 18 h of laser exposure. In these experiments, the laser spot was defocused to enlarge the spatial extent of the modified area. The spot size was measured separately. It was equal to  $1.5\text{ }\mu\text{m}$  and hence the laser irradiated area can be spatially resolved with confocal Raman spectroscopy. A complete Raman spectrum was recorded for each location (step size 200 nm in both spatial directions) and the intensity was evaluated for the three peaks. Apart from the inevitable blurring due to the diffraction limit, the modifications in the Raman spectrum are indeed spatially confined to the laser spot size.

## VI. ATOMIC FORCE MICROSCOPY

### A. Height study

A more accurate estimate of the affected region can be obtained by recording the topography with atomic force microscopy. To minimize the influence of the tip, such measure-

ments were performed in tapping mode. Figure 6(a) depicts an AFM image of a freshly prepared monolayer. The measured height of the flake is about 1 nm instead of 0.335 nm expected for a monolayer. This discrepancy has been reported previously and is attributed to adsorbed molecules on top of the graphene surface or in between the graphene layer and the substrate.<sup>27</sup> Note that in the tapping mode the AFM “height” may also contain a chemical contrast contribution. After laser exposure the irradiated region shows an additional even higher elevation of approximately 1.5 nm [Fig. 6(b)]. The disruption of carbon-carbon bonds offers additional docking sites for adsorbates. We associate this height increase with the adsorption of additional molecules from ambient air when the laser is turned off. This assertion is proved in transport experiments described in Sec. VII.

### B. Time dependence of the topography

To gain more insight into the topographical changes as the single graphene flake is decomposed into nanocrystallites, we have performed time-resolved AFM measurements. One way to do this would be to irradiate the flake with laser light for a certain time interval, obtain an AFM image, and continue with the laser irradiation at the same location. To circumvent the potential influence of the AFM tip, we have chosen a different route. Multiple spots, spatially apart by a sufficiently large distance to ensure no mutual influence, were irradiated with the laser for different time intervals. The laser power was set at 12 mW in all cases. After all spots were “written,” just a single AFM image was recorded in tapping mode. The AFM image is depicted in Fig. 7(a). The results of the image analysis are summarized in Figs. 7(b) and 7(c). In panel b, the diameter of the modified area is plotted as a function of the exposure time. The modification occurs first in the middle, where the laser intensity has its maximum. After 1 h, the modified area has grown into an area equal in size to the focused, diffraction-limited laser spot. The modified region does not expand further at longer exposure times. Also addressed in Fig. 7(c) is the time evolution of the height of the modified region. The indicated height is obtained from a histogram which plots the counts for each height contour. During the first 10 min, there is a slight decrease in the height. This corresponds to the removal of adsorbates initially present on the pristine flake. We note that a chemical contrast contribution may be contained in tapping mode images and hence when we refer to a change in height it also includes a potential change in the chemical contrast. The height decrease fits well with the observed redshift of the Raman  $G$  and  $2D$  peaks. Subsequently, the height increases as the crystalline flake is locally converted into a nanocrystalline network. As time progresses,  $sp^2$  carbon-carbon bonds are broken up. These broken bonds provide additional docking sites for molecular adsorbates such as water from the ambient atmosphere. That additional adsorbates appear after laser treatment is unambiguously confirmed in field-effect experiments which will be described in Sec. VII below. The increase in height is attributed to these additional adsorbates. It is well-known that it is not possible to properly identify monolayers, bilayers, or multilayers of graphene us-

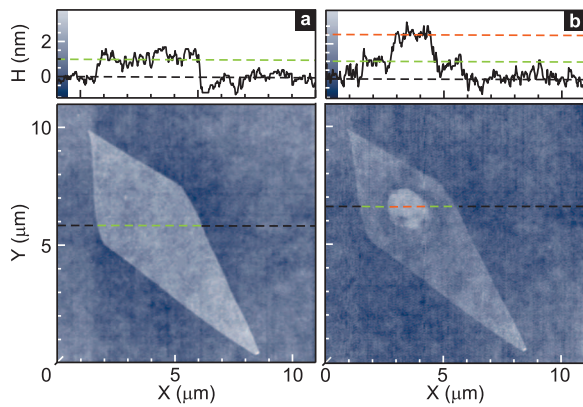


FIG. 6. (Color) AFM image of a graphene monolayer before and after laser exposure recorded in tapping mode. (a) AFM height image of a pristine graphene flake. The top panel shows a height scan along the dashed line. The height  $H$  of the substrate and the graphene surface are marked by the dashed black and green lines, respectively. The measured height difference is approximately 1 nm. (b) AFM height image after exposing one spot on the sample for 14 h with a 1 mW defocused 488 nm laser beam. An elevated area has appeared where the laser spot was positioned. In the top panel, the red dashed line marks its height. The difference with respect to the pristine graphene surface is approximately 1.5 nm. The diameter of the modified region coincides with the diameter of about 1.5  $\mu\text{m}$  of the defocused laser spot.

ing AFM images. The height of a monolayer of graphene (identified unequivocally using optical contrast, Raman spectroscopy or magnetotransport) typically ranges from 0.8–1.3 nm in an AFM image even though the actual graphene layer thickness is only 0.33 nm. Adsorbates on top of the flake or in between the substrate and the flake are held responsible for the discrepancy between the measured height and the true graphene thickness.<sup>27</sup> Hence, it is plausible to attribute the height increase upon laser irradiation to the larger number of attached adsorbates seen in field-effect studies. The height increase eventually slows down or terminates. This saturation coincides with the Raman data in which the  $D$  peak intensity no longer increases. No additional defects, i.e., broken bonds, are created. Hence, the accumulation of additional adsorbates stops and the height remains nearly constant. Note that the time scale for saturation in Fig. 7 is much shorter than for instance in Fig. 2, because the sample was irradiated with 12 mW of laser power instead of 1 mW for the data acquired in the experiment of Fig. 2.

### C. Topography near graphene edge

To evince that the observed changes in AFM images (increased height) and the Raman measurements are intimately connected with the presence of graphene, we have irradiated a graphene flake near its edge so that laser light is simultaneously incident on graphene and an uncovered piece of the  $\text{SiO}_2$  substrate. The edge region was exposed to 12 mW of laser light for 1 h. Figure 8 displays the AFM image after irradiation. On the bare  $\text{SiO}_2$  substrate, laser irradiation has little influence. A slight decrease in height is visible in the irradiated region. Presumably this is due to the removal of

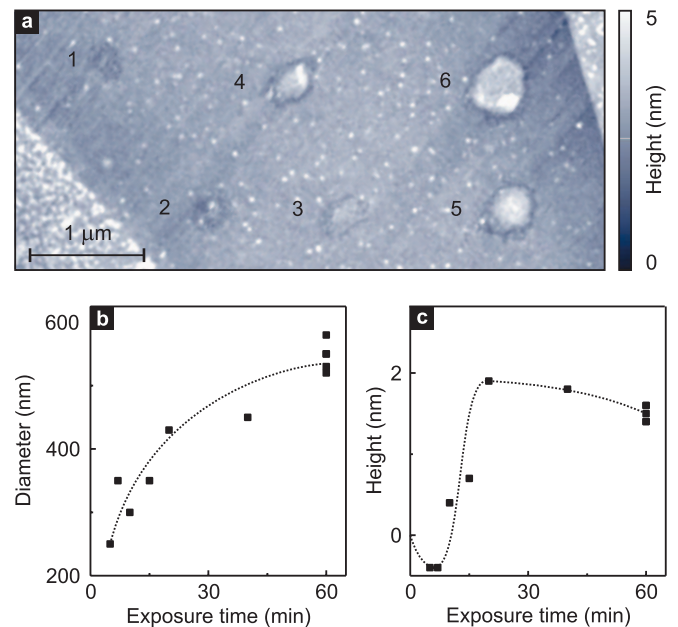


FIG. 7. (Color) AFM measurement on a graphene flake on which multiple laser spots with different exposure time have been written. (a) Height image of the laser treated areas. Laser treated areas are numbered. A large number corresponds to a longer exposure time. (b) Analysis of the diameter of the laser treated spots in (a). The modification of graphene occurs first in the middle of the laser spot where the laser intensity has its maximum. (c) Analysis of the height as a function of the exposure time. After a small decrease in height (removal of dopants) the height grows until it reaches a maximum. The increased height is attributed to the attachment of ambient species after the laser has been turned off.

molecular adsorbates. Even when irradiating the bare substrate for a much longer time period, no increase in height is observed. On the graphene flake however, the height has increased due to the gradual disassembly of crystalline graphene and the adsorption of a larger number of molecules. The border of the graphene flake does not wash out, instead the sharp boundary to the uncovered  $\text{SiO}_2$  substrate is maintained. For the sake of comparison, we show on the left side of Fig. 8 the disk shape which forms when the laser light is entirely incident on the graphene monolayer.

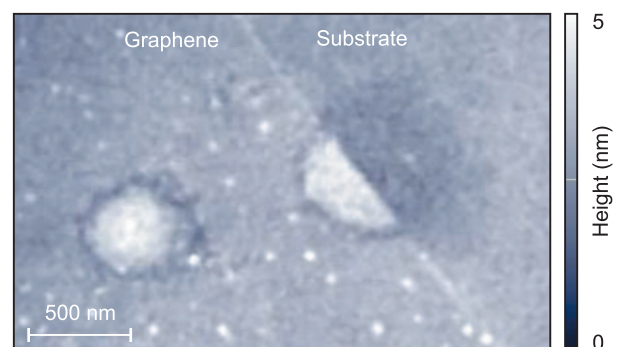


FIG. 8. (Color) AFM image of a flake which has been treated by laser light at the edge. Only the graphene itself shows an elevated height. For the sake of comparison also a spot located entirely within the flake has been “written.”

## VII. TRANSPORT CHARACTERISTICS AFTER LASER TREATMENT

It is well-known from noncontact scanning force microscopy studies<sup>28</sup> that on graphite crystals water nanodroplets preferably attach to steps. The laser treatment of graphene creates many additional edges (see the  $D$  peak behavior in Figs. 1, 2, and 4). They provide additional docking sites for instance for water droplets from the surrounding ambient air. Also other constituents from the surrounding atmosphere (e.g.,  $O_2$ ) may attach to the flake. Water as well as oxygen transfer charge and act as  $p$ -type dopants on graphene. This  $p$ -type doping can be observed experimentally by recording the field-effect transport curves after different times of laser irradiation. Field-effect data were recorded after the laser was switched off for 60 s.

Figure 9(a) shows an AFM image of a typical device used for recording these field-effect characteristics. The bright stripes are the Cr/Au contacts, the dark brown color is the  $SiO_2$  substrate. At the end of each contact lead, the AFM image is brighter, because in these regions the graphene monolayer is located underneath. This causes a slight height increase. The width of the contacts as well as the distance between adjacent contacts is approximately 600 nm. The incident laser beam has been schematically included as a transparent blue ray. Prior to modifying the flake we acquired a scanning confocal laser image, which enables us to position the laser spot precisely on the graphene in between the contacts.

The four terminal longitudinal resistance is plotted as a function of the applied back-gate voltage in Fig. 9(b) with the laser irradiation time as the parameter. A laser power of 12 mW has been used in this experiment. For short exposure times, the removal of the dopants which were already present on the as prepared flake dominates. It appears as a large shift of the charge neutrality point to smaller back-gate voltages during the first 20 min (faster than for Fig. 2 as a result of the increased laser power). The amount of boundary, i.e., the number of broken  $sp^2$  carbon-carbon bonds continuously increases with time. This enhances the reactivity. After switching off the laser, dopants easily attach to the flake and  $p$  dope it. After 7 h, the charge neutrality point is already higher than 60 V when the laser is switched off. By pumping and heating the dopants can be removed again and the charge neutrality point returns to lower back-gate voltages. Subsequent exposure to ambient air shifts the charge neutrality point reversibly back to the high doping state. This controlled enhancement of the reactivity of nanocrystalline graphene may be helpful to trim or tune for instance the properties of graphene based gas sensors.<sup>29</sup> It can also be exploited to generate spatially varying doping patterns.

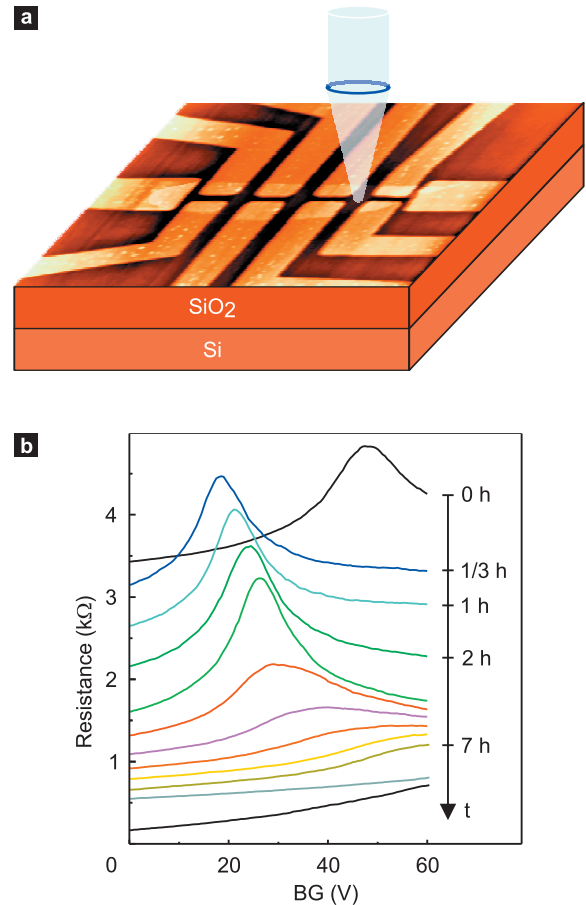


FIG. 9. (Color) Field-effect curves recorded on a graphene flake which has been exposed to laser irradiation. (a) AFM image of a typical device. (b) Field-effect characteristics for different laser exposure times. Before recording this transport data, the laser was switched off for 60 s. The removal of the dopants on the as prepared flake causes an initial shift of the charge neutrality point to lower back voltages, i.e., drop in the carrier concentration (first 20 min). As  $sp^2$  bonds get cracked, the reactivity of graphene is locally enhanced and more dopants from the ambient can adsorb after the laser light has been switched off. This results in an increase of  $p$ -type doping.

## VIII. SUMMARY

In summary, we have demonstrated that laser irradiation of graphene can be invasive and may induce controllable structural modifications. Long laser exposure locally disassembles a single crystalline layer of graphene into a network of interconnected graphene nanocrystallites. Their characteristic size saturates at approximately 10 nm in the limit of long exposure times. The additional boundaries provide docking sites for molecular adsorbates, so that the reactivity can be locally enhanced.

\*Present address: Eindhoven University of Technology, Mechanical Engineering, PO Box 513, WH 3.122, 5600 MB Eindhoven, The Netherlands

†j.smet@fkf.mpg.de

- <sup>1</sup>K. S. Novoselov, A. K. Geim, S. V. Morozov, D. Jiang, Y. Zhang, S. V. Dubonos, I. V. Grigorieva, and A. Firsov, *Science* **306**, 666 (2004).
- <sup>2</sup>M. A. Pimenta, G. Dresselhaus, M. S. Dresselhaus, L. G. Cançado, A. Jorio, and R. Saito, *Phys. Chem. Chem. Phys.* **9**, 1276 (2007).
- <sup>3</sup>A. C. Ferrari and J. Robertson, *Phys. Rev. B* **61**, 14095 (2000).
- <sup>4</sup>J. Yan, Y. Zhang, P. Kim, and A. Pinczuk, *Phys. Rev. Lett.* **98**, 166802 (2007).
- <sup>5</sup>F. Tuinstra and J. L. Koenig, *J. Chem. Phys.* **53**, 1126 (1970).
- <sup>6</sup>L. G. Cançado, R. Beams, and L. Novotny, arXiv:0802.3709 (unpublished).
- <sup>7</sup>L. G. Cançado, M. A. Pimenta, B. R. A. Neves, M. S. S. Dantas, and A. Jorio, *Phys. Rev. Lett.* **93**, 247401 (2004).
- <sup>8</sup>A. C. Ferrari *et al.*, *Phys. Rev. Lett.* **97**, 187401 (2006).
- <sup>9</sup>P. Blake, E. W. Hill, A. H. C. Neto, K. S. Novoselov, D. Jiang, R. Yang, T. J. Booth, and A. K. Geim, *Appl. Phys. Lett.* **91**, 063124 (2007).
- <sup>10</sup>S. Reich and C. Thomsen, *Philos. Trans. R. Soc. London, Ser. B* **362**, 2271 (2004).
- <sup>11</sup>C. Thomsen and S. Reich, *Phys. Rev. Lett.* **85**, 5214 (2000).
- <sup>12</sup>A. C. Ferrari, *Solid State Commun.* **143**, 47 (2007).
- <sup>13</sup>S. A. Solin and A. K. Ramdas, *Phys. Rev. B* **1**, 1687 (1970).
- <sup>14</sup>K. N. Kudin, B. Ozbas, H. C. Schniepp, R. K. Prud'homme, I. A. Aksay, and R. Car, *Nano Lett.* **8**, 36 (2008).
- <sup>15</sup>M. Hulman, M. Haluska, G. Scalia, D. Obergfell, and S. Roth, *Nano Lett.* **8**, 3594 (2008).
- <sup>16</sup>S. Pisana, M. Lazzeri, C. Casiraghi, K. S. Novoselov, A. K. Geim, A. C. Ferrari, and F. Mauri, *Nature Mater.* **6**, 198 (2007).
- <sup>17</sup>A. Das *et al.*, *Nat. Nanotechnol.* **3**, 210 (2008).
- <sup>18</sup>C. Casiraghi, S. Pisana, K. S. Novoselov, A. K. Geim, and A. C. Ferrari, *Appl. Phys. Lett.* **91**, 233108 (2007).
- <sup>19</sup>Z. H. Ni, T. Yu, Z. Q. Luo, Y. Y. Wang, L. Liu, J. M. Miao, W. Huang, and Z. X. Shen, *ACS Nano* **3**, 569 (2009).
- <sup>20</sup>S. Berciaud, S. Ryu, L. E. Brus, and T. F. Heinz, *Nano Lett.* **9**, 346 (2009).
- <sup>21</sup>C. Stampfer, F. Molitor, D. Graf, K. Ensslin, A. Jungen, C. Hierold, and L. Wirtz, *Appl. Phys. Lett.* **91**, 241907 (2007).
- <sup>22</sup>A. C. Ferrari and J. Robertson, *Phys. Rev. B* **64**, 075414 (2001).
- <sup>23</sup>P. Yu and M. Cardona, *Fundamentals of Semiconductors* (Springer, New York, 1999).
- <sup>24</sup>A. Singha and A. Roy, *Rev. Adv. Mater. Sci.* **10**, 462 (2005).
- <sup>25</sup>J. Maultzsch, S. Reich, C. Thomsen, H. Requardt, and P. Ordejón, *Phys. Rev. Lett.* **92**, 075501 (2004).
- <sup>26</sup>M. Lafkioti, B. Krauss, T. Lohmann, K. v. Klitzing, and J. H. Smet (unpublished).
- <sup>27</sup>M. Ishigami, J. H. Chen, W. G. Cullen, M. S. Fuhrer, and E. D. Williams, *Nano Lett.* **7**, 1643 (2007).
- <sup>28</sup>M. Luna, J. Colchero, and A. M. Baró, *J. Phys. Chem. B* **103**, 9576 (1999).
- <sup>29</sup>F. Schedin, A. K. Geim, S. V. Morozov, E. W. Hill, P. Blake, M. I. Katsnelson, and K. S. Novoselov, *Nature Mater.* **6**, 652 (2007).